

Femtosecond synchronism of x rays to visible light in an x-ray free-electron laser

Bernhard W. Adams^{a)}

Argonne National Laboratory, Argonne, Illinois 60439

(Received 19 November 2004; accepted 28 March 2005; published online 20 May 2005)

A way is proposed to obtain intense infrared/visible light from an electron bunch in an x-ray free-electron laser in femtosecond synchronism with the x-rays themselves. It combines the recently proposed technique of emittance slicing in a free-electron laser with transition undulator radiation (TUR). The part of the electron bunch that is left unspoiled in the emittance slicing process is the source of both coherent x rays and of coherent TUR at near-infrared wavelengths. An extension of the concept also exploits the fact that the electrons that participate in the free-electron lasing process lose a significant part of their energy. © 2005 American Institute of Physics. [DOI: 10.1063/1.1927109]

I. INTRODUCTION

The most elementary processes of chemistry and solid-state dynamics take place on the femtosecond time scale (corresponding to the electron-volt energies of chemical bonds) and on the angstrom length scale, corresponding to the interatomic distances. These time and length scales can be addressed in pump-probe experiments, where a femtosecond pulse of visible or infrared light triggers a process whose dynamics are probed by a correspondingly short x-ray pulse. The x rays can provide both the spatial resolution corresponding to the chemical bond lengths and, through near-edge spectroscopy, element-specific chemical information, such as the oxidation state of a particular elemental species.

Whereas the production of few-femtosecond, intense pulses of laser light is routine these days, the possibility of obtaining intense x rays of similar duration is only now appearing on the horizon. Laser-plasma x-ray sources have a low brilliance, and the duration of the x-ray pulses is of the order of 100 fs. The raw output from an x-ray free-electron laser (XFEL) is much more brilliant but of similar duration. Several schemes have been proposed in the past few years to obtain shorter x-ray pulses from a FEL. However, to obtain a few-femtosecond time resolution in a visible pump, x-ray probe experiment, one also has to determine the relative timing of the two types of radiation at a commensurate level of precision. It is very difficult to synchronize a short-pulse laser to the electron bunches in a linear-accelerator-driven XFEL to better than ~ 1 ps. A way to circumvent the problem is to measure the relative timing of the laser versus the electrons or the x rays on a shot-by-shot basis and to bin the data accordingly. This requires sophisticated crosscorrelation techniques, none of which are proven yet. It would also be very desirable to replace the statistical coverage of the pump-probe time difference with controlled and scanable femtosecond-precise timing. For this, pump and probe light have to be derived from the same source, i.e., the electrons in

the accelerator. One possible way for doing so is proposed here. It is based on a recent proposal to shorten the duration of FEL emission from an electron bunch by passively slicing its emittance. This has the advantage of requiring only minimal upgrades to an existing FEL facility and, in particular, does not need an additional drive laser. The current proposal combines this with the use of coherent transition undulator radiation (CTUR), i.e., transition undulator radiation¹ (TUR), enhanced by the effect of coherent synchrotron radiation (CSR). Transition undulator radiation is strongly peaked in the forward direction at an angle of $1/\gamma$, where γ is the relativistic electron energy in rest energy units. This makes TUR depend very sensitively on the emission angle. Correspondingly, the CTUR emission will be determined by the variations along the bunch of the electron density over the transverse angular coordinates in phase space. For few-femtosecond slices in the electron bunch, the CTUR appears in the near-infrared wavelength range.

Two concepts are proposed here. The first relies directly on the transverse emittance characteristics of an emittance-sliced bunch and the other works by transforming the energy spread of the sliced bunch into an angular spread in a bending magnet. The latter concept can be extended to also make use of the energy loss of the electrons that participate in the free-electron lasing process. The next section describes the concept in qualitative terms. The numbers given are based upon the simulations² and parameters available from the linac coherent light source (LCLS) parameter database.

II. EMITTANCE SLICING

In the emittance-slicing technique,² a thin foil is placed in a bunch compressor at a point where an energy chirp in the bunches is transformed into a transverse spread. As the electrons traverse the foil, they are scattered and their transverse and longitudinal emittances are increased by roughly one order of magnitude each. An aperture in the foil leaves a small part of the bunch near its center largely unaffected (apart from insignificant wakefield effects). Only this central

^{a)}Electronic mail: adams@aps.anl.gov

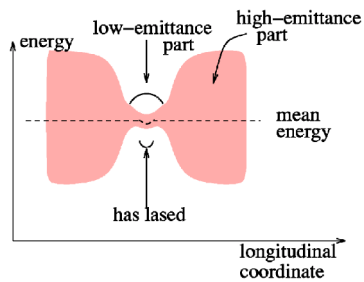


FIG. 1. (Color online) Schematic representation of the particle energy, mean and spread, along an emittance-sliced bunch as it leaves the FEL undulator. The parts of the bunch that passed through the foil have a larger energy spread than the central part that was left unaffected. In the center of the unaffected part, the electrons have participated in the SASE emission and have a lower mean energy than those in the rest of the bunch.

part has a low enough emittance to be able to support the self-amplified spontaneous emission (SASE) process that leads to the emission of highly intense x rays in the LCLS and similar x-ray FELs. Due to slippage effects,² the free-electron-lasing part of the bunch is even shorter than the unspoiled part itself. The electrons that participate in the emission of the intense coherent laser radiation lose a significant fraction of their energy (see Sec. IV). They also lose energy to incoherent emission of wiggler radiation (with the current LCLS parameters actually considerably more than to coherent emission). However, this loss is the same as in the emittance-spoiled part of the bunch because (i) spontaneous emission is a single-electron effect and therefore the total radiated power is independent of the bunch emittance, and (ii), at least in the linear-gain section of the FEL, the Fourier components of the electron density are not coupled with each other, so that gain in those that fulfill the undulator resonance condition does not affect the other ones.

After leaving the undulator, the bunch consists thus of several distinct regions: (i) the center, which has participated in the SASE process (henceforth the SASE bunch), surrounded by (ii) regions of unspoiled emittance, which have not lased, and (iii) the head and tail regions, which have large longitudinal and transverse emittances. Due to the additional energy loss to coherent radiation, the electrons in the SASE bunch have a slightly lower mean energy than the others. This is shown schematically in Fig. 1. With the exception of the central dip due to energy transfer into the coherent x rays, a plot of the transverse emittance of the electrons looks qualitatively similar.

In the following Secs. III and IV, two concepts for the extraction of infrared CTUR from an emittance-sliced bunch are described. The first (Sec. III) seems rather simple to implement. The other is more complex and requires some more space in the XFEL facility, but could provide shorter wavelength CTUR than the first.

III. USE OF TRANSVERSE EMITTANCE

In the LCLS, $\gamma=26\,693$, and the emission of TUR peaks at the small angle of $1/\gamma=37\ \mu\text{rad}$ (see Fig. 2). In contrast, the source size $\sigma=\gamma\lambda/2$ that emits into one transverse mode of the infrared radiation with this high collimation ($\sigma\approx 13\ \text{mm}$ at $\lambda=1\ \mu\text{m}$) is much larger than the electron beam

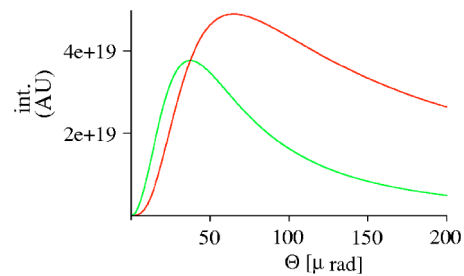


FIG. 2. (Color online) Dependence of the TUR intensity from the LCLS undulator on the observation angle Θ at $\lambda=1\ \mu\text{m}$. Lower curve: into a constant solid angle [Eq. [1].(11)], upper curve: into a constant interval in Θ , integrated over the azimuthal angle. For the lower curve, the units on the abscissa represent the photon flux at $\lambda=1\ \mu\text{m}$ per second, mrad^2 and 0.1% bandwidth at a beam current of 5 kA. For the upper curve, the units are arbitrary.

cross section in the LCLS undulator, and, therefore, the emission of TUR is insensitive to emittance-induced electron beam cross section variations. As a consequence of the large transverse source size, the electron beam must follow a straight path over a long distance of the order of a hundred meters (see Appendix C). Thus, the place in the LCLS that suggests itself for the production of TUR is the main undulator itself, which in the current design is 112 m long.

CSR effects are caused by strong variations of the electromagnetic field amplitude *at the observation point*, which are due to variations in the phase-space density along the bunch. In the case of a bending magnet, it is usually sufficient to consider only the overall charge-density variations along the bunch, and a qualitative understanding of CSR can be found by concentrating on the bunch itself. With TUR, however, the location of the observation point becomes important for two reasons. First, the high degree of collimation of TUR makes the amplitude at the observation point depend on only that fraction of the bunch charge whose propagation direction is within an angle of $1/\gamma$ of the direction towards the observation point (see Fig. 3). A formal definition of a directional charge density is given in Eq. (B2). The second difference to bend magnet CSR is that the observer is typically in the near field of the TUR source (see Appendix C).

In the LCLS design,³ the normalized slice emittance $\gamma\epsilon$ is $1.2\times 10^{-6}\ \text{m}$, and the average β function in the LCLS undulator is $23\ \text{m/rad}$, giving a root-mean-square transverse beam size $\sqrt{\beta\epsilon}=36\ \mu\text{m}$, and a divergence of $1.25\ \mu\text{rad}$.

With the parameters given in Ref. 2, the spoiled transverse emittance is about $5\times 10^{-6}\ \text{m}$, or about four times higher than the unspoiled emittance according to the LCLS database³ and about six times the unspoiled value of $0.8\ \mu\text{m}$ given in Ref. 2. In either case, the resulting increase in the electron beam divergence to $\sim 2.5\ \mu\text{rad}$ and $3\ \mu\text{rad}$, respectively, is still much less than the TUR peaking angle. As Fig. 4 shows, this is not sufficient for a good contrast in the directional electron density. The increased divergence can, however, be amplified by placing one or more scattering foils at the undulator entrance, and making use of the fact that, along with an about twofold increase in divergence, there is also a twofold increase in the transverse size of the spoiled beam. Each of the foils has a hole that is just large enough to let the unspoiled beam pass. The foils must be spread out

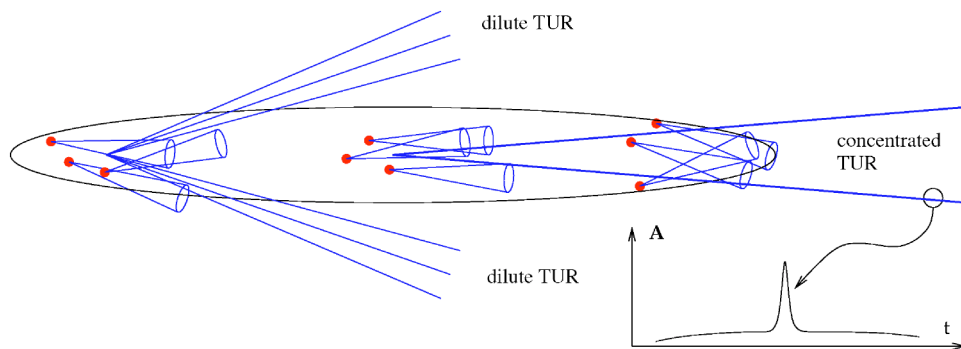


FIG. 3. (Color online) Schematic representation of the variations in the divergence along the bunch. The center has a smaller electron divergence, and thus a smaller TUR divergence, than the head (light rays not drawn) or the tail (divergent light rays shown). The inset shows the amplitude A over the time t at the location of the observer. Short-wavelength CTUR is due to the square of the peak over the slow pedestal.

over a length given by the β function to make sure that all electrons in the spoiled parts interact with several foils, i.e., those that happen to be close to the beam center at the first foil must interact with another. Other than in the beam compressor, where the original emittance slicing foil is placed, there is no dispersion at the undulator entrance, and therefore, the limitations on the total foil thickness discussed in Ref. 2 do not apply. However, possible wakefield effects of the foils on the unspoiled beam need to be studied in beam-dynamic simulations. To increase the divergence of the spoiled beam to, say, $60 \mu\text{rad}$, the emittance will have to be increased by a factor of about 2000. Assuming uncorrelated scattering in the foils, the emittance should scale linearly with the total foil thickness. According to Ref. 2, $10 \mu\text{m}$ of carbon increases the emittance by a factor of 5, and thus, a total foil thickness of 4 mm will be required (but see remark at the end of this section). Going downstream, the foils can have increasing aperture size, as the distinction between spoiled and unspoiled parts grows. This will help to minimize adverse wakefield effects on the unspoiled part of the bunch. Depending on the emittance acceptance of the LCLS, the foils will also scatter some electrons completely out of the beam, so that not only the directional, but also the total, electron density of the spoiled parts is reduced by the scattering. This effect may actually be more important than that due to only the reduction in directional emittance. To avoid damage to the undulator, the scattered electrons should be caught by a collimating beam stop.

Figure 5 shows a sketch of the proposed device, with the primary scattering foil sf_1 in the bunch compressor and sf_2 representing the multiple emittance-enhancing foils. In an actual design, one would probably not use foils with an aperture, but rather several blades that can be moved into the beam from all sides. The TUR in Fig. 5 is focused onto the sample by a long (several meters, depending on the imaging

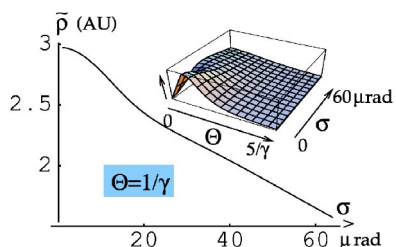


FIG. 4. (Color online) Main graph: Square of the directional electron density $\bar{\rho}$, Eq. (B2) for an observation angle $\Theta = 1/\gamma = 37 \mu\text{rad}$ over the electron beam divergence σ . Inset: the same over σ and Θ .

ratio) parabolic mirror. Because of the radial polarization of the TUR light [see remark after Eq. (A9)], focusing the whole emission cone onto the sample would lead to destructive interference. Therefore, one can use only about $1/3$ of the cone to get an optical single-cycle burst of infrared radiation (one-half cycle of the vector potential) or two opposing sections of the cone with a $\lambda/2$ phase shifter for a $3/2$ -cycle burst (one full cycle of the vector potential). The x rays go through two crystal reflections for the double purpose of monochromatization and delay relative to the infrared light (see Ref. 4 for details).

Now to the intensity of CTUR light that one may expect at the important wavelength of $\lambda = 800 \text{ nm}$, for which the mature Ti:sapphire laser technology is available. This also is the wavelength below which the Taylor expansion for the exponential (A5) becomes invalid for LCLS parameters ($K = 3.5$, $\gamma = 26693$, undulator length $L = 112 \text{ m}$). The number of TUR photons from a single electron at an angle $\Theta = 1/\gamma$ is calculated with Eq. (B3). Assuming the observer is several hundred meters downstream of the undulator, the real undulator length L is replaced with an effective $L^\circ = 100 \text{ m}$ to account for near-field effects (see Appendix A). With $\omega = 2\pi c/\lambda = 2.355 \times 10^{15} \text{ s}^{-1}$ and $\Delta\omega = 0.2 \cdot \omega$ (typical for Ti:sapphire), and with $\langle \beta_\perp^2 \rangle = K^2/4\gamma^2 \approx 4.3 \times 10^{-9}$, this gives $dN/d\Omega = 3.0 \times 10^5$. After integrating over a solid angle of γ^{-2} ($0.5/\gamma$ radially and 2γ azimuthally), the flux is $N = 4.21 \times 10^{-4}$ photons from one electron.

According to the simulation in Ref. 2, the beam current in the unspoiled part is 6 kA, and thus the charge transport within one-half optical oscillation period of 800 nm light is 8 pC, or 4.9×10^7 electrons. Because CTUR scales as the square of the number n of participating charges and because the contrast C between $\bar{\rho}^2$ (see Fig. 4 and the inset in Fig. 3) in the unspoiled versus the spoiled part is about 50%, the CTUR pulse energy is $N \cdot n^2 \cdot \hbar\omega C \approx 125 \text{ nJ}$, and the power within one optical cycle is about 50 MW. This is quite sufficient for many pump-probe experiments. If necessary, stan-

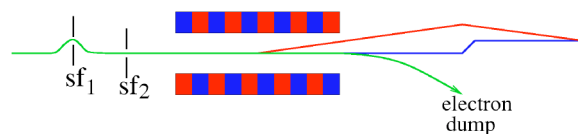


FIG. 5. (Color online) Schematic of the in-line setup, with the scattering foil sf_1 , as proposed in Ref. 2, and the additional foils at location sf_2 . The x rays go through a double-bounce monochromator, which has the secondary purpose of delaying them relative to the CTUR light.

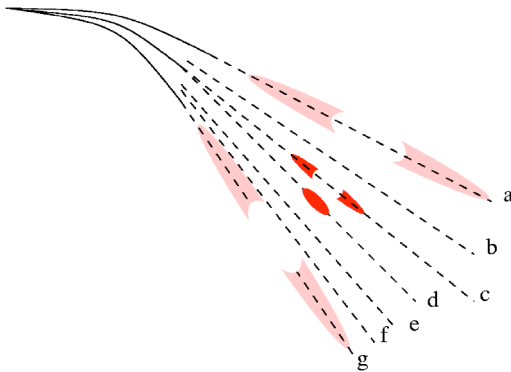


FIG. 6. (Color online) Schematic representation of the time dependences in the dispersed bunch after the bend. The high-emittance parts of the bunch spread out over a large fan, represented here by trajectories *a*, *b*, *e*, *f*, and *g*. In all of these trajectories, the low-emittance central part of the bunch is missing because that is concentrated on the trajectories *c* (has not lased) and *d* (has lased). The electrons that participate in the SASE process lose more of their initial energy than those that do not, and therefore take a tighter turn in the bend and end up in trajectory *d*, instead of *c*.

ard laser technology can be used for further amplification: a single pass through a laser crystal in in-line geometry introduces only a small optical delay, which can easily be compensated for with an x-ray delay in the monochromator. Finally, a laser amplifier could also be used to reduce the requirements on the contrast in $\tilde{\rho}$ between the spoiled and unspoiled parts of the bunch and thus use fewer secondary scattering foils.

IV. USE OF THE ENERGY SPREAD

The second concept makes use of the variation of the energy spread along the bunch. Upon entering the dipole magnet that separates the electrons from the x rays to send them to the beam dump, the bunch fans out, and the regions with a large energy spread do so much more than those that were left unaffected by the emittance slicing. Furthermore, the parts of the unaffected region that have/have not lased will follow different trajectories due to their slightly different mean energies. This is shown schematically in Fig. 6.

This dispersed bunch then enters another undulator, which has the purpose of emitting infrared CTUR (see Fig. 7). There, the current density profile shown in Fig. 6 will lead to the following pattern of CTUR emission at micrometer wavelengths (given by the duration of the emittance-sliced SASE emission): the main component due to the short SASE bunch is centered around trajectory “*d*.” In this direction, one should observe a single optical cycle of infrared light (a half-cycle of the vector potential). On trajectory “*c*,”

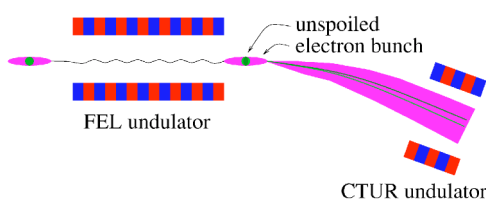


FIG. 7. (Color online) A sketch of the setup, showing the FEL undulator, the bend magnet that disperses the bunch and the undulator for transition undulator emission.

there is a somewhat longer bunch, corresponding to the total duration of the unspoiled section, but with a “hole” in its center where the electrons go along ‘*d*’. In analogy to Babinet’s principle in classical optics, this should also lead to CTUR at the same wavelength as from *d*. Because the parts of the bunch on ‘*c*’ before and after the hole are roughly equal in length to the hole itself, one may expect a $1\frac{1}{2}$ -cycle pulse of the vector potential. Finally, there are the outer trajectories “*a*,” “*b*,” “*e*,” “*f*,” “*g*.” These contain rather long bunches which emit CTUR at far-infrared wavelengths, albeit rather weakly because their currents are more dilute than on ‘*c*’ and ‘*d*’. Furthermore, for the same reason as discussed earlier, there is also a weak CTUR contribution at wavelengths corresponding to the length of the bunch on ‘*c*’.

The CTUR must be produced in a straight section of about 100 m in length (see Appendix C), but the total undulator length can be less. One might, for example, array relatively short undulators along the long straight section. These undulators do not have to conform to the strict tolerances of the SASE undulator in the LCLS. Because $\langle\beta_{\perp}\rangle$ enters Eq. (B3) to the fourth power, a shorter magnetic length can easily be made up for by a larger *K* parameter of the undulator (see remark in Appendix A on $K > 1$ and the TUR peaking angle of $1/\gamma$).

Now to an estimate of the CTUR power to be expected: According to the LCLS database,³ the energy spread of the unspoiled part of the bunch before the emission of x rays is 0.01%, and the quantum fluctuations of the spontaneous wiggler radiation induce an additional spread of 0.02%, bringing the total to 0.024%. In contrast, the emittance of the spoiled parts of the bunch is about 0.075%.² The relative energy loss due to the SASE process is about 0.014% with a coherent x-ray power of 10 GW from a current of 5 kA of 13.64 GeV electrons. In the LCLS design,³ the bend magnet leading to the beam dump consists of three sections, each with a magnetic length of 1.4 m and a deflection angle of 1.67° . The total deflection from all three dipole magnets is thus $5^{\circ} = 88$ mrad, and the energy spreads of 0.024% and 0.075% fan out over 21 and 66 μ rad, respectively. According to Fig. 4, this gives a contrast in $\tilde{\rho}$ of about 30% (2.4 in arbitrary units at 21 μ rad to 1.55 at 66 μ rad). With undulator parameters similar to those of the LCLS (or, alternatively, shorter undulator section with higher *K*), the CTUR pulse energy is then of the order of 0.1 μ J (see power estimates in Sec. III). A stronger or longer bending magnet would improve the contrast. One might also use secondary scattering foils, as discussed in Sec. III to increase the energy spread of the spoiled parts and thus increase the contrast in $\tilde{\rho}$.

The energy loss of 0.014% due to the SASE process leads to an angular deviation of 12 μ rad, which is about 1/3 of the peaking angle $\Theta = 1/\gamma$ of the TUR. Even without any energy spread in the SASE bunch, this gives a very small contrast in $\tilde{\rho}$ (see Fig. 4). With the 0.024% energy spread of the SASE bunch, this contrast is decreased even further. However, the coherent x-ray power of 10 GW is an average value. The SASE radiation exhibits very strong intensity fluctuations, and, in some bunches, the power loss to coherent x-ray emission is much larger—a factor of 2 will improve the contrast in $\tilde{\rho}$ to about 10%. This also opens the interest-

ing possibility of using the CTUR as a diagnostic tool to monitor the energy loss to coherent x-ray emission independently from the x rays themselves.

ACKNOWLEDGMENTS

This work was supported by the U.S. Department of Energy, Office of Basic Energy Sciences under Contract No. W-31-109-ENG-38. Thanks also to Paul Emma at SLAC and Kwang-Je Kim and Eric Landahl of Argonne National Lab for their comments and suggestions. The author would also like to thank the reviewer for carefully reading of the manuscript and spotting a numerical error.

APPENDIX A: NEAR-FIELD TUR

This Appendix revisits the derivations of the original paper¹ on TUR for an undulator that is not negligibly short in comparison to the observation distance, i.e., near-field TUR.

The electromagnetic field of a relativistic electron traversing an undulator of length L in a time $T=L/c$ is observed at a point \mathbf{x} relative to the origin placed into the center of the undulator. The momentary position of the electron is $\mathbf{r}(t)$, and $\boldsymbol{\beta}(t)$ is its velocity in units of the speed of light. Because later on, a bunch of electrons will be considered, \mathbf{r} must be split into the position \mathbf{r}_0 of the bunch center and the position \mathbf{s} of the electron relative to \mathbf{r}_0 . Beam-dynamic effects will not be considered, i.e., \mathbf{s} is assumed constant and $\mathbf{r}(t) = \mathbf{r}_0(t) + \mathbf{s}$. The coordinate origin is chosen in the center of the undulator and $\mathbf{r}_0(0) = \mathbf{0}$.

The vector from the electron to the observer is $\mathbf{R}(t) = \mathbf{x} - \mathbf{r}(t)$, expressed in terms of the distance $R(t) = |\mathbf{R}(t)|$ and direction $\mathbf{n}(t) = \mathbf{R}(t)/R(t)$. The angle Θ of observation is given by $\cos \Theta = \mathbf{n} \cdot \mathbf{r}(t)/|\mathbf{r}|$. This geometry is shown in Fig. 8.

With Eqs. (14.62) and (14.66) of Ref. 5, the vector potential observed at position \mathbf{x} is

$$\mathbf{A}(\omega) = \left(\frac{e^2}{8\pi^2 c} \right)^{1/2} \int_{-T/2}^{T/2} e^{i\omega(t+R(t)/c)} \frac{d}{dt} \left[\frac{\mathbf{n} \times [\mathbf{n} \times \boldsymbol{\beta}]}{1 - \boldsymbol{\beta} \cdot \mathbf{n}} \right] dt, \quad (\text{A1})$$

where integration limits $\pm\infty$ of Eq. (14.62) of Ref. 5 are replaced with $\pm T/2$ under the assumption that the electrons go on straight paths before and after the undulator. This assumption and the minimum lengths of these paths are discussed in Appendix C.

Because γ is very large in the LCLS, the observation angle Θ is small (see later) and the length of the undulator producing the TUR (see Appendix C) is a sizeable fraction of the overall dimensions of the XFEL facility. Therefore, \mathbf{n} cannot be taken as a constant, and the common approximation (14.63) of Ref. 5 $R(t) = |\mathbf{x}| - \mathbf{n} \cdot \mathbf{r}(t)$ must be examined for its validity. This makes it necessary to revisit the derivations of Ref. 1.

With the law of cosines, $\mathbf{x}^2 = \mathbf{r}^2 + R^2 + 2|\mathbf{r}|R \cos \Theta(t)$, a quadratic equation for R is obtained, which can be solved as

$$R \approx |\mathbf{x}| - \mathbf{n} \cdot \mathbf{r} - \frac{\mathbf{r}^2}{2|\mathbf{x}|} + \frac{(\mathbf{n} \cdot \mathbf{r})^2}{2|\mathbf{x}|} (1 + \mathbf{r}^2/\mathbf{x}^2) \quad (\text{A2})$$

by expanding the square root to first order. Keeping only the terms $|\mathbf{x}|$, $\mathbf{n} \cdot \mathbf{r}$ and the next-order corrections, realizing $|\mathbf{s}| \ll |\mathbf{r}|$, and using $\mathbf{r}^2 - (\mathbf{n} \cdot \mathbf{r})^2 = \mathbf{r}^2 \sin^2 \Theta$, gives

$$R \approx |\mathbf{x}| - \mathbf{n} \cdot \mathbf{r} - \mathbf{n} \cdot \mathbf{s} - \frac{\mathbf{r}^2 \sin^2 \Theta}{2|\mathbf{x}|}, \quad (\text{A3})$$

and, with $\kappa(t) = 1 - \mathbf{n} \cdot \boldsymbol{\beta}$ and the approximations $|\mathbf{r}| \approx ct$ and $\sin \Theta \approx \Theta$, the exponential in Eq. (A1) becomes

$$\Phi \phi(\mathbf{s}) \exp \left[i\omega \int_0^t \kappa(t') dt' - i\omega \frac{ct^2 \Theta^2}{2|\mathbf{x}|} \right], \quad (\text{A4})$$

where $\Phi = \exp(i\omega|\mathbf{x}|/c)$ and $\phi(\mathbf{s}) = \exp(-i\omega\mathbf{s} \cdot \mathbf{n}/c)$ are both constant in time. The former, Φ , is of no further concern here because \mathbf{x} is constant. The latter, ϕ , is also constant in time and thus irrelevant here. However, it will be all-important in Appendix B in the context of coherent synchrotron radiation.

With $\mathbf{n} \cdot \boldsymbol{\beta} = \cos \Theta |\boldsymbol{\beta}|$ and $|\boldsymbol{\beta}| = \sqrt{1 - \gamma^{-2}}$, we have $\kappa \approx (\gamma^{-2} + \Theta^2)/2$, and with $\mathbf{n} \times \boldsymbol{\beta} \approx \sin \Theta$, the expression in the square brackets in Eq. (A1) peaks at $\Theta = 1/\gamma$. The observation point \mathbf{x} will have to be chosen accordingly, and sections of the undulator for which Θ deviates strongly from $1/\gamma$ contribute only weakly. At $\Theta = 1/\gamma$, the integral in the argument of the exponential in Eq. (A4) is larger than the fraction following it by a factor of $2|\mathbf{x}|/ct$, and can be written as

$$\exp \left[i\omega \int_0^t \sigma(t') \kappa(t') dt' \right], \quad \sigma(t) = 1 - \frac{ct}{|\mathbf{x}|}. \quad (\text{A5})$$

As long as the argument of that exponential is much smaller than $\pi/2$, the scaling factor σ may be considered a small quantitative correction, not leading to qualitatively significant changes in interference effects. Also, in that case, the exponential in Eq. (A5) may be written as a Taylor expansion to first order. With $\Theta = 1/\gamma = 37 \mu\text{rad}$ and an undulator length of 100 m, the limiting wavelength, below which the exponential exceeds unity, is about 800 nm.

After writing $\mathbf{A}(\omega) = (e^2/2c)^{1/2} \Phi \phi \mathcal{A}(\omega)$ to make the following derivations directly comparable to Ref. 1, and performing an integration by parts, we get an expression corresponding to Eq. (2) of Ref. 1:

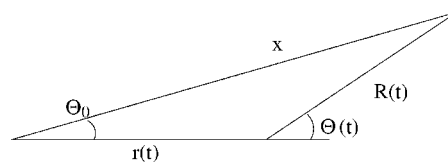


FIG. 8. Geometry of the determination of $R(t)$ and $\mathbf{n}(t)$.

$$\mathcal{A}(\omega) = \frac{1}{2\pi} \left\{ \left[1 + i\omega \int_0^t \sigma(t') \kappa(t') dt' \right] \times \left[\frac{\mathbf{n} \times [\mathbf{n} \times \boldsymbol{\beta}(t)]}{\kappa(t)} \right] \Big|_{-\frac{T}{2}}^{\frac{T}{2}} - \int_{-T/2}^{T/2} \frac{\mathbf{n} \times [\mathbf{n} \times \boldsymbol{\beta}(t)]}{\kappa(t)} i\omega \sigma(t) \kappa(t) dt \right\}. \quad (\text{A6})$$

Under the assumption that the velocity loss and directional change in the undulator is negligible, i.e., $\boldsymbol{\beta}(-T/2) = \boldsymbol{\beta}(T/2) =: \boldsymbol{\beta}_0$ and $\kappa(-T/2) = \kappa(T/2) =: \kappa_0$, this is

$$\mathcal{A}(\omega) = \frac{i\omega}{2\pi} \int_{-T/2}^{T/2} \sigma(t) \times \frac{\mathbf{n} \times (\mathbf{n} \times \boldsymbol{\beta}_0) \kappa(t) - \mathbf{n} \times [\mathbf{n} \times \boldsymbol{\beta}(t)] \kappa_0}{\kappa_0} dt. \quad (\text{A7})$$

With the explicit representation $\kappa(t) = 1 - \mathbf{n} \cdot \boldsymbol{\beta}(t)$ and the vector formula $\mathbf{a} \times (\boldsymbol{\beta} \times \mathbf{c}) = (\mathbf{a} \cdot \mathbf{c}) \boldsymbol{\beta} - (\mathbf{a} \cdot \boldsymbol{\beta}) \mathbf{c}$ (applied to both double cross products and, again, for assembly), Eq. (A6) becomes

$$\mathcal{A}(\omega) = \frac{i\omega}{2\pi} \int_{-T/2}^{T/2} \sigma(t) \left\{ \frac{\mathbf{n} \times [\mathbf{n} \times (\boldsymbol{\beta}_0 - \boldsymbol{\beta})]}{\kappa_0} + \frac{\boldsymbol{\beta}_0(\boldsymbol{\beta} \cdot \mathbf{n}) - \boldsymbol{\beta}(\boldsymbol{\beta}_0 \cdot \mathbf{n})}{\kappa_0} \right\} dt. \quad (\text{A8})$$

The electron velocity consists of a rapid transverse oscillation $\boldsymbol{\beta}_\perp$ and a longitudinal oscillation about an average longitudinal velocity $\boldsymbol{\beta}_\parallel \approx \mathbf{e}_\ell (|\boldsymbol{\beta}_0| - \langle \boldsymbol{\beta}_\perp^2 \rangle / 2)$, where, for the purposes of considering a single electron, the vector $\mathbf{e}_\ell = \boldsymbol{\beta}_0 / |\boldsymbol{\beta}_0|$ can be considered to be identical to the unit vector \mathbf{e}_z . The transverse velocity $\boldsymbol{\beta}_\perp$ is given by $|\boldsymbol{\beta}_\perp| = (K/\gamma) \cos(2\pi ct/\lambda_u)$, where K is the undulator parameter ($K=3.5$ in the LCLS), and λ_u is the undulator period in the lab frame. The transverse oscillation and, to a much lesser extent, the longitudinal oscillation are the source of the regular undulator radiation at high frequencies. These rapid oscillations average out in the integration in Eq. (A8) because that expression has been derived with a first-order Taylor expansion for the exponential in Eq. (A5). This expansion would clearly be invalid in a derivation of the regular undulator radiation because the whole point of using an undulator is to introduce a phase slippage of many times 2π . This also brings up another point: at first sight, it may seem contradictory to predict a peaking of TUR at $\Theta = 1/\gamma$ when the angular variations of the electron trajectory exceed this angle at $K > 1$. However, here too, one has to distinguish between the average longitudinal velocity and the high-frequency wiggles, whose effect averages out in the integration.

Therefore, the second fraction in Eq. (A8), whose numerator is $[\boldsymbol{\beta}_0(\boldsymbol{\beta}_\perp \cdot \mathbf{n}) - \boldsymbol{\beta}_\perp(\boldsymbol{\beta}_0 \cdot \mathbf{n})] \approx -\boldsymbol{\beta}_\perp$, does not contribute, and of $\boldsymbol{\beta}_0 - \boldsymbol{\beta}$ in the first fraction, only $\langle \boldsymbol{\beta}_\perp^2 \rangle / 2$ remains.

$$\mathcal{A}(\omega) = \frac{i\omega}{2\pi} \int_{-T/2}^{T/2} \sigma(t) \mathbf{n} \times (\mathbf{n} \times \mathbf{e}_\ell) \frac{\langle \boldsymbol{\beta}_\perp^2 \rangle}{2\kappa_0} dt. \quad (\text{A9})$$

Due to the term $\mathbf{n} \times (\mathbf{n} \times \mathbf{e}_\ell)$, the TUR light is radially polarized. If the factor $\sigma(t) = 1$, and with a constant angle Θ [hidden in $|\mathbf{n} \times (\mathbf{n} \times \mathbf{e}_\ell)| = \sin \Theta$], Eq. (A9) could be integrated trivially and Eq. (10) of Ref. 1 would be obtained. However, for observation distances $|\mathbf{x}|$ not much larger than the undulator length, the factor $\sigma(t)$ drops off from 1 for times t corresponding to the ends of the undulator and $\Theta(t)$ deviates from the peaking value of $1/\gamma$ for at least some parts of the undulator (see Fig. 8). Both σ and Θ thus have the effect of restricting the length of the undulator that actually contributes to an effective length $L^\circ < L = Tc$.

When observed at the angle $\Theta = 1/\gamma$, the frequency range $\omega_\ell < \omega < \omega_u$ of the radiation is bounded below by the reciprocal relativistically compressed effective undulator traversal time. The upper limit ω_u is given by the condition that the exponent in Eq. (A5) must be small.

APPENDIX B: CTUR

Instead of a single electron, we shall now consider an electron bunch with a phase-space density $\rho(z, \beta, x, x', y, y')$, where the longitudinal coordinate z and the transverse spatial and angular coordinates x, y and x', y' are meant relative to the bunch center. The density ρ is normalized to make the integral over X equal to the number of electrons in the bunch. The validity of this continuous-density model is discussed later. In the context of a bunch, the phase factor $\phi(\mathbf{s}) = \exp(i\omega \mathbf{s} \cdot \mathbf{n}/c)$ becomes relevant. It can be approximated by $\exp(i\omega z/c)$ because \mathbf{n} is almost parallel to the z axis.

With Eq. (14.60), of Ref. 5 the number N of photons emitted into a frequency band $\omega \pm \Delta\omega/2$ and into a solid angle $d\Omega$ is $d^2N/d\omega d\Omega = 2|\mathcal{A}(\omega)|^2/\hbar\omega$, and thus

$$\frac{dN}{d\Omega} = \frac{\Delta\omega}{\omega} \alpha \left| \int dX \rho(X) e^{ikz} \mathcal{A}(\omega) \right|^2, \quad (\text{B1})$$

where $k = \omega/c$, $\alpha = e^2/\hbar c$, and X is an abbreviation for the set of arguments to ρ .

The energy spread in the bunch is assumed to be so small that γ and $\boldsymbol{\beta}_\perp$ can be taken as constants. However, the beam divergence is important here, and the vector \mathbf{e}_ℓ can no longer be assumed to be parallel to \mathbf{e}_z . Taking the coordinate direction \mathbf{x} to be in the plane of \mathbf{n} and \mathbf{e}_z , the expression $|\mathbf{n} \times (\mathbf{n} \times \mathbf{e}_\ell)|$ is now $|\Theta - \mathbf{x}'|$, where \mathbf{x}' is the two-dimensional vector of the transverse angular coordinates (x', y') and Θ is the observation angle, also as a two-dimensional vector. Likewise, in the denominator $2\kappa_0 = 2(1 - \mathbf{n} \cdot \boldsymbol{\beta}) \approx (\Theta^2 + \gamma^{-2})$ must now be replaced with $[(\Theta - \mathbf{x}')^2 + \gamma^{-2}]$, and, with this, the term $[\mathbf{n} \times (\mathbf{n} \times \mathbf{e}_\ell)]/(2\kappa_0)$ in Eq. (A9) is now modified to read $(\Theta - \mathbf{x}')/[(\Theta - \mathbf{x}')^2 + \gamma^{-2}]$. Multiplying this with $\rho(X)$, and performing the trivial integrations over β, x, y (which do not appear in the integrand) gives the definition

$$\tilde{\rho}(z, x', y') = \frac{\gamma^{-1} |\Theta - \mathbf{x}'|}{(\Theta - \mathbf{x}')^2 + \gamma^{-2}} \int d(\beta, x, y) \rho(X), \quad (\text{B2})$$

which can be interpreted as the directional electron density, radiating towards the observer. The units of $\tilde{\rho}$ are number-of-

electrons per real-space volume. With this, Eq. (B1) is

$$\frac{dN}{d\Omega} = \frac{\alpha\omega\Delta\omega L^{\circ 2}\gamma^2\langle\beta_{\perp}^4\rangle}{4c^2\pi^2} \times \left[\int dz_1 dz_2 d\mathbf{x}'_1 d\mathbf{x}'_2 e^{ik(z_1-z_2)} \times \tilde{\rho}(z_1, x'_1) \tilde{\rho}(z_2, x'_2) \right]. \quad (\text{B3})$$

The subscripts 1, 2 are used to differentiate between integration variables instead of the customary prime “ \prime ” to avoid confusion with the notation of angular variables.

With $\tilde{\rho}$ being a number density per real-space volume, the integral in Eq. (B3) is dimensionless. The units in the fraction before the integral cancel out, leaving a dimensionless number N of photons per unit solid angle Ω . The integral can be interpreted as representing the number of charges correlated with each other on the scale of the wavelength $\lambda = 2\pi/k$ in z and within an (x, y) divergence of $1/\gamma^2$. If the directional charge density exhibits strong variations in z within the wavelength λ , coherent synchrotron radiation effects appear, which are proportional to $\tilde{\rho}^2$ in the respective volume, i.e., the square of the number of participating charges.

A caveat: At very low charge densities, when the mean distance in z between electrons within a (x, y) divergence of $1/\gamma^2$ is not much smaller than λ , the electron density $\tilde{\rho}$ must be made to reflect the quantized nature of the electric charge. This can be done through the introduction of statistical fluctuations in $\tilde{\rho}$ smaller than λ in longitudinal extent. Otherwise, Eq. (B3) would give unphysical results: in the extreme case of one electron in a bunch many times the length of λ , a smoothly spread-out electron density would make the double integral be much less than $\gamma^{-2}\Theta^2/(\Theta^2 + \gamma^{-2})^2$ (as it should be for a point charge). With typical XFEL parameters, i.e., 1 nC in a bunch of 30 μm in length and at micron wavelengths, this problem does not occur. For the comparison of the CTUR intensity to that due to TUR from a single elec-

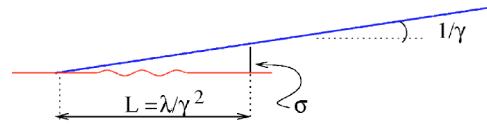


FIG. 9. (Color online) The minimum length of the straight section containing the undulator is determined by the source size σ due to diffraction of the infrared light of wavelength λ .

tron, the integral in Eq. (B3) can be replaced with $\gamma^{-2}\Theta^2/(\Theta^2 + \gamma^{-2})^2$, which makes Eq. (B3) correspond to Eq. (11) of Ref. 1.

APPENDIX C: RADIATION LENGTH

An important implicit assumption in the above treatment of TUR is that the electrons enter and leave the undulator on extended straight paths. Just how long these straight sections have to be can be determined through a consideration of the coherence characteristics of the emitted TUR (see Fig. 9). Corresponding to the small peaking angle $\Theta = 2/\gamma$ of the azimuthally integrated emission (see Fig. 2), the transverse source size is given by $\sigma = \lambda/(2/\gamma)$. The observer that sees this transverse size at an angle of $2/\gamma$ is actually looking at a straight section of length $L = \sigma/(2/\gamma) = \gamma^2\lambda/4$, which contains the TUR-emitting undulator. At a wavelength of $\lambda = 800$ nm (the wavelength of Ti:sapphire lasers) and with the LCLS value of $\gamma = 26\,693$, the straight section must be at least $L = 145$ m long, i.e., a bit more than the length of the LCLS undulator (112 m)! Any bends or other deviations from a perfectly straight electron path within this length will generate radiation that interferes with the TUR, which will generally have the effect of increasing the solid angle into which the radiation is emitted.

¹K.-J. Kim, Phys. Rev. Lett. **76**, 1244 (1996).

²P. Emma, K. Bane, M. Cornacchia, Z. Huang, H. Schlarb, G. Stupakov, and D. Walz, Phys. Rev. Lett. **92**, 074801 (2004).

³LCLS parameter database, URL <http://www-ssrl.slac.stanford.edu/lcls/parameters.html>.

⁴B. Adams, Rev. Sci. Instrum. **75**, 1982 (2004).

⁵J. Jackson, *Classical Electrodynamics*, 2nd ed. (Wiley, New York, 1975).